Chen, Ruiying; Martin, Floran; Li, Yongjian; Yue, Shuaichao; Belahcen, Anouar

An Energy-Based Anisotropic Vector Hysteresis Model for Rotational Electromagnetic Core Loss

Published in:
IEEE Transactions on Industrial Electronics

DOI:
10.1109/TIE.2023.3294635

Published: 01/01/2023

Document Version
Peer-reviewed accepted author manuscript, also known as Final accepted manuscript or Post-print

Please cite the original version:
Chen, R., Martin, F., Li, Y., Yue, S., & Belahcen, A. (2023). An Energy-Based Anisotropic Vector Hysteresis Model for Rotational Electromagnetic Core Loss. *IEEE Transactions on Industrial Electronics*, 1-11. Article 10188384. https://doi.org/10.1109/TIE.2023.3294635

An Energy-based Anisotropic Vector Hysteresis Model for Rotational Electromagnetic Core Loss

Ruiying Chen, Floran Martin, Yongjian Li, Shuaichao Yue, and Anouar Belahcen, *Senior Member, IEEE*

***Abstract*—In this paper a model that describes the anisotropic behavior and core loss of electrical steel sheets over a wide range of rotational excitation is developed. Based on the definition of the effective field, the macroscopic anisotropy field is deduced from a weighted average of the magnetocrystalline energy of a single crystal. An anisotropic vector hysteresis model is then proposed by applying the effective field to the energy-based model. Experimental measurements are used to fit and validate the model. Either alternating or rotational measurements with a maximum magnetic flux density 1.55 T under 10 Hz are employed to fit the model parameters and the remaining set of measurements is used for validating the model accuracy. The results show that the model can naturally account for the drop in the rotational losses at high flux densities regardless of whether it is identified from alternating or rotational measurement data. The generality of the model is demonstrated through continuous angle results and modeling of another material.**

***Index Terms*—Electrical steel sheets, magnetic anisotropy, vector hysteresis, rotational core loss.**

I. Introduction

ELECTRICAL steel sheets are widely used in electromagnetic devices such as machines and transformers. The research shows that there are rotational magnetization in the cores of these devices, resulting in large rotational loss [1], [2]. Using hysteresis model to characterize magnetic properties is an effective loss prediction method [3]. In order to improve the loss calculation accuracy of electromagnetic devices, the vector magnetic properties of electrical steel sheets and the related models should be adequately developed and implemented. Hence, the modeling approach should consider the hysteresis and the anisotropy phenomena. These two properties are known to vary with the magnitude of the excitation, making it a challenging task to propose an accurate and computationally efficient vector hysteresis model.

Manuscript received Month xx, 2xxx; revised Month xx, xxxx; accepted Month x, xxxx. This work was supported in part by the National Natural Science Foundation of China under Grant 52130710; in part by the Funds for Creative Research Groups of Hebei Province under Grant E2020202142, in part by "S&T" Program of Hebei under Grant 20311801D, and in part by the State Scholarships Fund of China No. 202006700007. (Corresponding author: Yongjian Li)

Ruiying Chen, Yongjian Li and Shuaichao Yue are with the State Key Laboratory of Reliability and Intelligence of Electrical Equipment, Hebei University of Technology, Tianjin 300130, China (e-mail: 201911401010@stu.hebut.edu.cn; liyongjian@hebut.edu.cn; 201811401006@stu.hebut.edu.cn).

Floran Martin, Anouar Belahcen and Ruiying Chen are with the Department of Electrical Engineering and Automation, Aalto University, Espoo FI-00076, Finland (e-mail: floran.martin@aalto.fi; anouar.belahcen@aalto.fi).

Many hysteresis models have been proposed and developed into anisotropic models. Mayergoyz vectorized the scalar Preisach model by projecting the input to different redundant directions and superposing the outputs of these directions calculated by a scalar model [4]. The approach is mathematically rigorous, but resulted in a physically incorrect behaviour of the losses at high values of the rotating flux density, i.e., the losses do not drop at these values as observed in many experiments. To overcome this problem, other researchers added exponential and phase shift terms to the expression of projection to consider the anisotropy, but these developed models reproduce inaccurately the change of anisotropy with the amplitude of magnetization. Alternatively, the vector properties can be modeled in spite of an excessive computational effort for the parameter identification [5], [6]. There is a vector Preisach model that can simulate the rotational loss by the transformation of variables, whereas it is isotropic [7]. The hybrid vector models, on the other hand, are based on the vector hysterons and the probability densities of these hysterons. For example, the direction and magnitude of magnetization are computed by the Stoner-Wohlfarth model and Preisach model, respectively, is known as Preisach-Stoner-Wohlfarth (PSW) model [8], [9]. However, the Preisach model involved in the above approach has the problem that parameter identification too complex, and many researchers are still working on optimizing its identification process [10], [11]. The Della Torre-Pinzaglia-Cardelli model defines the hysteron by an equipotential surface on the field plane to leverage the complexity of the PSW model. In this model, the change of magnetization state occurs only when the applied field is outside the equipotential surface [12]. Besides, some literature analyzes energy from the micromagnetics field and establishes macroscopic models to characterize the heterogeneity and multi-axiality of the material behaviour, called multi-scale models [13], [14]. As for purely numerical modeling of anisotropic hysteresis, the model proposed by Enokizono and Soda is a typical one, whereas it contains many parameters and requires large amounts of experimental data during the identification process [15].

A feasible and efficient method to consider anisotropy is decomposing the applied field into the irreversible and reversible field and modifying the isotropic vector model into an anisotropic one from these two aspects. The coenergy model extracts the vector anhysteretic curves from the measured data to construct the equipotential surfaces of coenergy density, then predicts the magnetic properties by calculating the derivative of coenergy density [16], [17]. As for the vector Jiles-Atherton (JA) model, one way to handle the anisotropy is to take the interpolated anhysteretic surface from the alternating measurements in different directions [18]. The spline interpo-

lation used in this model is more accurate than the traditional Langevin function but it contains much more parameters. Another approach is separate the model parameters into the rolling direction (RD) and transverse direction (TD) parts [19]. The parameters of this model vary with the amplitude of the magnetic flux density, which does not meet the requirements of complex and variable excitation in engineering. Among this type of models, the energy-based (EB) model combines the advantages of both the JA model and Preisach model [20], [21]. This model has an energy interpretation of the magnetic material's behavior. Its vector hysteron represents magnetic hysteresis as a friction-like force to calculate the reversible field. The radius of one hysteron is regarded as the pinning force of the domain. The magnetization is assumed to be aligned with the reversible field and its value is obtained by an anhysteretic function with respect to the reversible field. Furthermore, the outputs of all hysterons are summed by probability densities, which yields the ability to predict the hysteresis loops with different sizes. Such a model is worth further developing as what is done in this paper.

The current anisotropic EB model has two versions. One consists in separating the parameters into two orthogonal directions and superposing the outputs of these two directions [22]. In this model, the radius and probability densities of the hysterons are obtained by an auxiliary function, which is identified from the measured coercive field. The other version consists in replacing the scalar magnetic reluctivity of the anhysteretic curve with a tensorial one, and modifying the circular hysteron to an ellipse [23]. However, these methods do not solve the specific property of rotational magnetization which consists in the drop of rotational loss when the sample is magnetized close to saturation. In this situation, the coherent rotation is the dominant magnetization process. The current method to make the EB model accounts for the coherent rotation property is to shrink the radius of hysterons with the increase of the applied field, which is an effective mathematical correction [24]. A feasible and physically correct approach to consider the anisotropy and the coherent rotation would be to minimize the crystal energy with the support of the microscopic measurements and modelling [14], [25]. However, if a model is to be broadly applicable in engineering, it should mostly rely on macroscopic magnetic measurements.

In this paper, an energy-based anisotropic vector hysteresis model is proposed and its development is explained. Several innovations as listed below are introduced to achieve the required level of accuracy. Based on the single crystal theory, the total energy of the magnetized sample is derived by a rotation matrix and the expression of the effective field that can account for the material anisotropy is given. The macroscopic energy minimum of the sample are characterized in this method to avoid the microscopic measurements. A vector anhysteretic model is firstly proposed by using the effective field as the input. In this model, the magnetization is set aligned with the effective field and a double Langevin function is adapted to predict the amplitude of magnetization. Then the anhysteretic model is extended to a hysteretic model in the frame of the EB model. The direction of magnetization is adjusted to rotate between the direction of the reversible effective field and the direction of the effective field based on the energy minimum. The discrete probability density parameters of the original EB model, which is used to assemble all the hysterons are replaced by a tangent hyperbolic function (tanh) with only 2 parameters, which removes the discretization roughness. The identification procedure with either alternating or rotational flux measurements of non-oriented electrical steel sheets B35A210 is explained in detail, and the model is validated and shown to be accurate and physically meaningful. The fact that the model is physic-based releases the requirement on the identification procedure and makes it easier. The rest of the paper is organized as follows. In section II, the transition from the single crystal microstructure to the macroscopic behaviour is explained, followed by the development of the anhysteretic model and then the hysteretic model. The implementation methodology is also presented in this section. In section III the measurements are briefly presented, the identification procedure is explained and the simulation results for the magnetization and the core losses are presented for different identification loading cases. In section IV the ability of model to predict arbitrary angles behavior and another material is verified. A discussion and conclusion summarizing the results is also given at the end.

II. METHOD

A. The single crystal energy

In this subsection, the anhysteretic properties of the material and the derivation of the needed equations are first focused on. For this purpose, the approximate expression of the energy minimum of the sample is deduced based on the single crystal energy, and then the direction of the anhysteretic magnetization is determined accordingly. In the following subsections, the hysteresis model and the related concepts as well as the implementation methodology are then introduced.

The developed model is inspired by the actual microstructure of the material, the concepts needed to go from this microstructure to the macroscopic model are given here. When there is no spatial rotation and applied stress, the energy of a single crystal with magnetization direction $\boldsymbol{\gamma}_{\mathrm{c}}=[\gamma_1\,\gamma_2\,\gamma_3]^{\mathrm{T}}$ is:

$$W_{\mathrm{c}} = W_{\mathrm{hc}} + W_{\mathrm{anc}}. \tag{1}$$

W_{hc} is the magneto-static energy which comes from the applied field $\boldsymbol{H}$:

$$W_{\mathrm{hc}} = -\mu_0 m_{\mathrm{s}} \boldsymbol{H} \cdot \boldsymbol{\gamma}_{\mathbf{c}} \tag{2}$$

where μ_0 is the vacuum permeability and m_{s} the saturation magnetization. The easy axis is the direction in which a crystal is most easily magnetized. W_{anc} is the magnetocrystalline anisotropy energy that tends to force the magnetization to be aligned along the direction of the easy axis. It can be written in a general form:

$$W_{\mathrm{anc}} = \sum_{i,j,k}^{N_{\mathrm{p}}} k_{ijk} \gamma_1^i \gamma_2^j \gamma_3^k \tag{3}$$

where i, j and k are the power of γ_1, γ_2 and γ_3, respectively, and N_{p} is the maximum power of the polynomial decomposition. k_{ijk} are the polynomial coefficients. This equation can be

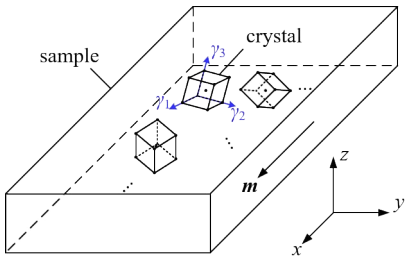

Fig. 1. Illustration of different crystal orientations in the polycrystalline sample.

used to express the anisotropic energy of any single crystal. In the case of the cubic symmetry, k_{220}=k_{022}=k_{202}=K_1, k_{222}=K_2. In the case of the uniaxial symmetry, k_{200}=K_u. K_1, K_2 and K_u are the magnetocrystalline anisotropy constants.

Similar to the applied field in (2), the effective field that can account for the anisotropic energy is defined as [26]:

$$\begin{aligned}\boldsymbol{H}_{\text{effc}} &= -\frac{1}{\mu_0 m_\text{s}}\frac{\partial W_\text{c}}{\partial \boldsymbol{\gamma_\text{c}}} \\ &= \boldsymbol{H} + \boldsymbol{H}_\text{anc}\end{aligned} \tag{4}$$

where the anisotropic field is

$$\boldsymbol{H}_\text{anc} = -\frac{1}{\mu_0 m_\text{s}}\frac{\partial W_\text{anc}}{\partial \boldsymbol{\gamma_\text{c}}}. \tag{5}$$

This definition of the effective field has its roots in the micromagnetism theory, where the orientation of every domain can be determined by solving $\boldsymbol{H}_{\text{effc}}\times\boldsymbol{\gamma_\text{c}}=\boldsymbol{0}$. The above equations will now be empowered to derive the anisotropic anhysteretic model, which is needed in the development of the hysteresis model.

B. Anhysteretic macroscopic model

To develop the anhysteretic model, the material sample is considered as a polycrystalline aggregate, which cannot be directly represented by a single crystal behaviour. However, for a sample with anhysteretic magnetization $\boldsymbol{M}_\text{anh}$=$M_\text{anh}\boldsymbol{e}_{\boldsymbol{M}\text{anh}}$, $\boldsymbol{e}_{\boldsymbol{M}\text{anh}}$=$[m_1\ m_2\ m_3]^\text{T}$, it can be treated as the assembly of cubic crystals as shown in Fig. 1. The directions $\boldsymbol{\gamma}_\text{c}$ of each crystal can be expressed in the sample coordinate system thanks to a rotation matrix $\boldsymbol{R}$ and the following transformation:

$$\boldsymbol{\gamma}_\text{c} = \boldsymbol{R}\cdot\boldsymbol{e}_{\boldsymbol{M}\text{anh}}. \tag{6}$$

Applying this transformation to (3) with the cubic symmetry case and taking into consideration the fact that the magnetic properties of the sample are symmetric, i.e., the expression of sample anisotropy energy W_an should be an even function of m_1, m_2 and m_3 simultaneously. In 2D case, m_3=0, then:

$$\begin{aligned}-\frac{W_\text{an}}{\mu_0 M_\text{s}} = {} & K_{40}m_1^4 + K_{04}m_2^4 + K_{60}m_1^6 + K_{06}m_2^6 \\ & + K_{22}{m_1}^2{m_2}^2 + K_{42}m_1^4m_2^2 + K_{24}m_1^2{m_2}^4\end{aligned} \tag{7}$$

where M_s is the saturation magnetization of the sample and the power of m_1 and m_2 in each term corresponds to the subscript of parameter K. The elements of matrix $\boldsymbol{R}$ are contained in K, while the values of $\boldsymbol{R}$ elements do not need to be obtained. The sum of the anisotropy energy of crystals in the sample gives the total anisotropy energy. The ratio of crystal with different magnetization directions is unknown, whereas the total anisotropy energy still has the form of the equation above. An expression of the anisotropic field $\boldsymbol{H}_\text{an}$ of the sample in 2D is derived as:

$$\begin{aligned}H_\text{anx} = {} & 4K_{40}m_1^3 + 2K_{22}m_1{m_2}^2 + 6K_{60}m_1^5 \\ & + 4K_{42}m_1^3m_2^2 + 2K_{24}m_1{m_2}^4 \\ H_\text{any} = {} & 4K_{04}m_2^3 + 2K_{22}m_1^2m_2 + 6K_{06}m_2^5 \\ & + 4K_{24}m_1^2m_2^3 + 2K_{42}m_1^4m_2\end{aligned}. \tag{8}$$

For the effective field of the sample, $\boldsymbol{H}_\text{eff}$, the anisotropic field should vanish at low applied field since the energy minimization leads to domains aligned with the easy direction. However, when the magnetization approaches saturation, the magnetic domains tend to be aligned with the applied field direction. To account for this domain rotation process, an anisotropic function $F(M_\text{anh}/M_\text{s})$ is used to modulate the field:

$$\begin{aligned}\boldsymbol{H}_\text{eff} &= -\frac{1}{\mu_0 M_\text{s}}\frac{\partial W}{\partial \boldsymbol{e}_{\boldsymbol{M}\text{anh}}} \\ &= \boldsymbol{H} + F\left(\frac{M_\text{anh}}{M_\text{s}}\right)\boldsymbol{H}_\text{an}\end{aligned} \tag{9}$$

where W is the energy of sample. $F(M_\text{anh}/M_\text{s})$ is chosen as

$$F\left(\frac{M_\text{anh}}{M_\text{s}}\right) = \frac{\left(1-\eta^3\right)\dfrac{M_\text{anh}}{M_\text{s}}}{1-\left(\eta\dfrac{M_\text{anh}}{M_\text{s}}\right)^3} \tag{10}$$

where η is a parameter in the range of (0,1). The characteristics that this function needs to satisfy are: its value range is (0,1), it is monotonically increasing, and its second derivative should be positive. Fig. 2 shows the shapes of it with different η.

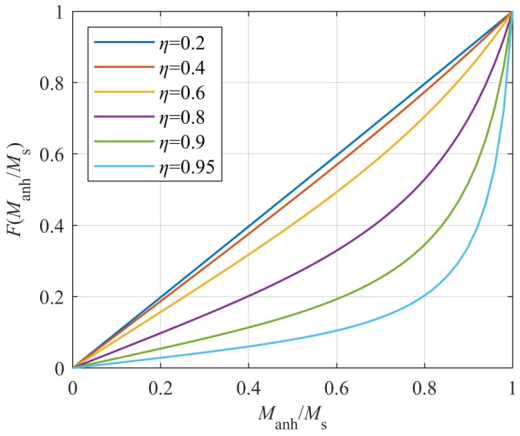

Fig. 2. Shape of the function $F(M/M_\text{s})$ for different values of the parameter η.

An anhysteretic macroscopic model is proposed based on (9). The input is $\boldsymbol{H}$ and the amplitude of $\boldsymbol{M}_\text{anh}$ is obtained by applying H_eff to the double Langevin function [27]

$$M_\text{anh} = M_\text{s}\left[\begin{array}{l}\omega\left(\coth\left(\dfrac{H_\text{eff}}{a_1}\right)-\dfrac{a_1}{H_\text{eff}}\right) \\ \\ +(1-\omega)\left(\coth\left(\dfrac{H_\text{eff}}{a_2}\right)-\dfrac{a_2}{H_\text{eff}}\right)\end{array}\right] \tag{11}$$

where a_1, a_2, ω and M_s are parameters that need to be identified. ω takes values from 0 to 1. To be consistent with

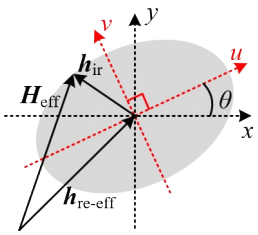

Fig. 3. Illustration of the elliptic hysteron used in the vector hysteresis model. θ is the orientation of the hysteron with respect to the x-axis.

the physical meaning of the effective field, that $\boldsymbol{H}_{\rm eff}\times\boldsymbol{e}_{\boldsymbol{M}\rm anh} = \boldsymbol{0}$, $\boldsymbol{M}_{\rm anh}$ is always aligned with $\boldsymbol{H}_{\rm eff}$:

$$\boldsymbol{e}_{\boldsymbol{M}\rm anh} = \boldsymbol{e}_{\boldsymbol{H}\rm eff}. \tag{12}$$

It should be mentioned that $\boldsymbol{H}_{\rm eff}$ depends on the direction of $\boldsymbol{M}_{\rm anh}$, making the correspondence of H-$M_{\rm anh}$ varies with the change of direction. Therefore, the scalar function (11) can be utilized rather than the vector anhysteretic surface extracted from the rotational measurements or the alternating measurements with different directions.

C. Vector hysteresis model

To account for the hysteresis within the framework of the EB model, the applied field $\boldsymbol{H}$ is decomposed into a reversible part $\boldsymbol{H}_{\rm re}$ and an irreversible part $\boldsymbol{H}_{\rm ir}$ [20]:

$$\boldsymbol{H} = \boldsymbol{H}_{\rm re} + \boldsymbol{H}_{\rm ir}. \tag{13}$$

In this method, it is the effective field $\boldsymbol{H}_{\rm eff}$ which is decomposed into a reversible effective field $\boldsymbol{H}_{\rm re\text{-}eff}$ and an irreversible field $\boldsymbol{H}_{\rm ir}$:

$$\boldsymbol{H}_{\rm eff} = \boldsymbol{H}_{\rm re\text{-}eff} + \boldsymbol{H}_{\rm ir}. \tag{14}$$

Therefore, the hysteresis and the anisotropy effects are both included in this model. In the implementation, a series of elliptical hysterons are adapted. For one hysteron illustrated in Fig. 3, half of the major axis is defined as κ and half of the minor axis is defined as $L\kappa$. The hysterons have the same rotation angle θ with respect to the x-axis. The surfaces of hysterons are where the Barkhausen jumps appear. The reversible effective field $\boldsymbol{h}_{\rm re\text{-}eff}$ and irreversible field $\boldsymbol{h}_{\rm ir}$ follow (14) and the unknown $\boldsymbol{h}_{\rm re\text{-}eff}$ at each calculation step is updated by

$$\boldsymbol{h}_{\rm re\text{-}eff} = \begin{cases} \boldsymbol{h}_{\rm re\text{-}eff} & |\boldsymbol{H}_{\rm eff} - \boldsymbol{h}_{\rm re\text{-}eff}| < h_{\rm ir} \\ \boldsymbol{H}_{\rm eff} - h_{\rm ir}\dfrac{\boldsymbol{H}_{\rm eff} - \boldsymbol{h}_{\rm re\text{-}eff}}{|\boldsymbol{H}_{\rm eff} - \boldsymbol{h}_{\rm re\text{-}eff}|} & |\boldsymbol{H}_{\rm eff} - \boldsymbol{h}_{\rm re\text{-}eff}| \geq h_{\rm ir} \end{cases} \tag{15}$$

The outputs of all hysterons are weighted by the probability densities function of the pinning sites, $p(\kappa)$, and summed together to obtain the total reversible effective field $\boldsymbol{H}_{\rm re\text{-}eff}$:

$$\boldsymbol{H}_{\rm re\text{-}eff} = \sum_{n=1}^{N_{\rm h}} \boldsymbol{h}_{\rm re\text{-}eff}^{n} \cdot p(\kappa_n) \tag{16}$$

where $N_{\rm h}$ is the number of hysterons.

On the basis of $\boldsymbol{H}_{\rm eff}$ and $\boldsymbol{M}_{\rm anh}$ determined by the anhysteretic model, the amplitude of the total magnetization $\boldsymbol{M}$ is computed by (11) with respect to $H_{\rm re\text{-}eff}$.

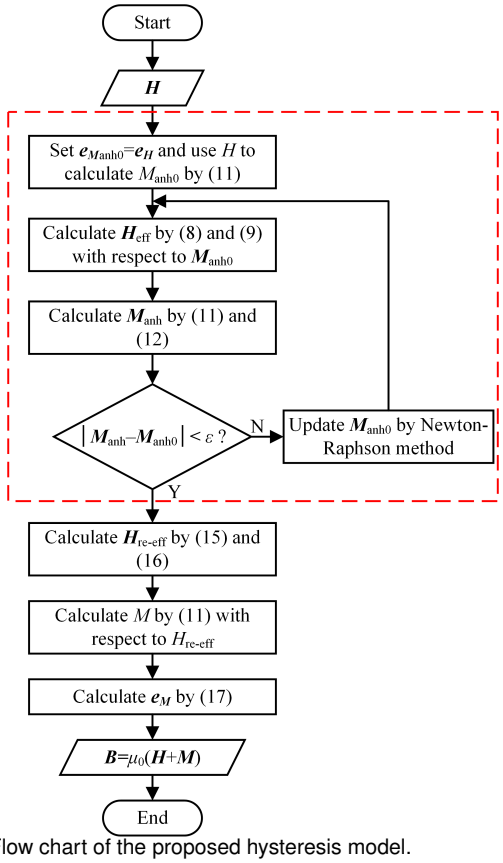

Fig. 4. Flow chart of the proposed hysteresis model.

The domain wall motion and Barkhausen jumps are already represented in this model. However, the coherent rotation should also be considered for the rotational magnetization. Hence, the direction of magnetization $\boldsymbol{e}_{\boldsymbol{M}}$ should rotate between the directions of $\boldsymbol{H}_{\rm re\text{-}eff}$ and $\boldsymbol{H}_{\rm eff}$. For this purpose, the same approach as for the anisotropy modeling is used, thus:

$$\boldsymbol{e}_{\boldsymbol{M}} = \left[1 - F\left(\frac{M_{\rm anh}}{M_{\rm s}}\right)\right]\boldsymbol{e}_{\boldsymbol{H}\rm re\text{-}eff} + F\left(\frac{M_{\rm anh}}{M_{\rm s}}\right)\boldsymbol{e}_{\boldsymbol{H}\rm eff}. \tag{17}$$

D. Implementation

Fig. 4 shows the calculation process of the proposed hysteresis model for one field step. First, the amplitude of the initial magnetization $\boldsymbol{M}_0$ is obtained according to the anhysteretic curve function (11) with respect to H. The direction of $\boldsymbol{M}_0$ is set to be equal to that of $\boldsymbol{H}$, considering the fact that there is not a big difference between them. Second, $\boldsymbol{H}_{\rm eff}$ and $\boldsymbol{M}_{\rm anh}$ are calculated iteratively with the Newton-Raphson method until the accuracy requirement $\epsilon = 1\times10^{-8}$ is fulfilled. The outputs of the elliptical hysterons (15) are then used to obtain $\boldsymbol{H}_{\rm re\text{-}eff}$ by (16). In the present implementation, 200 hysterons with κ_x were uniformly defined from 5 A/m to 1000 A/m. The $p(\kappa)$ in (16) is defined as

$$p(\kappa) = C_0\left[1 - \tanh\left(\frac{\kappa - C_1}{C_2}\right)\right] \tag{18}$$

where C_0, C_1 and C_2 are parameters. C_0 can be determined from $\sum p(\kappa) = 1$ while C_1 and C_2 should be determined from measurements. Finally, the magnetization is calculated by the obtained $\boldsymbol{H}_{\rm re\text{-}eff}$ and $\boldsymbol{H}_{\rm eff}$. The magnetic flux density $\boldsymbol{B}$ is the

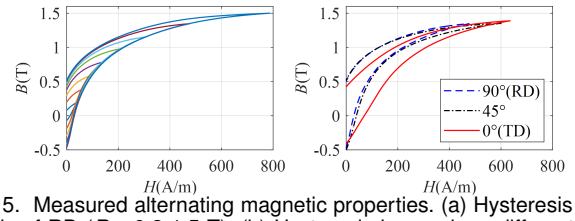

Fig. 5. Measured alternating magnetic properties. (a) Hysteresis loops family of RD ($\boldsymbol{B}_{\mathrm{p}}$=0.2-1.5 T). (b) Hysteresis loops along different magnetization directions ($\boldsymbol{B}_{\mathrm{p}}$=1.4 T).

final output of this model. The dashed box area in Fig. 4 is the proposed anhysteretic model, which can be used separately in some specific situations where only anhysteretic magnetic properties are required. In such a way, the implementation resulted in an average number of iterations required for each field step of less than 4.

III. Results

In this section, the results from both the measurements and the simulations are presented. The non-oriented electrical steel sheets B35A210 is utilized to verify the presented models. The thickness of sample is 0.35mm. Both the alternating and rotational magnetic properties are measured with the same device at a controlled waveform and frequency of the magnetic flux density of 10 Hz. The transverse direction (TD) of the sample is along the x-axis and the rolling direction (RD) is along the y-axis. A detailed description of the measurement setup and the approach followed hereinafter is given in [6].

The measurement data is decomposed into two sets, i.e., the alternating flux density data set, denoted as (A) in the following, and the rotational flux density data set denoted as (R). For both sets, $\boldsymbol{B}_{\mathrm{p}}$ denotes the amplitude of the magnetic flux density. Examples of dataset (A) are shown in Fig. 5, where the alternating flux density is applied at 0°, 45° and 90° directions with respect to the sample x-axis. Due to the symmetry of the data about the origin point, only images of the first and fourth quadrants are displayed. For each case, the amplitude of the flux density vary between about 0.2 and 1.55 T. For the rotational case, an example of the data set is shown Fig. 6, where only the measured $\boldsymbol{H}$ loci are shown, since $\boldsymbol{B}$ are controlled to be circular with the specified amplitudes. For the model validation purpose, the model parameters are identified either from the set (A) or the set (R) and the other set is used for validating and testing the model performances. Therefore, in the following, the parameters have the subscript A or R to indicate the data set used for the fitting procedure.

A. Identification procedure

In summary, the hysteresis model has 16 parameters: K_{40}, K_{04}, K_{22}, K_{60}, K_{06}, K_{42}, K_{24} and η to represent the anhysteretic anisotropy, a_1, a_2, M_{S} and ω to represent the anhysteretic curve, C_1 and C_2 to represent the probability density of the pinning sites, and L and θ to represent the shape and orientation of the hysterons. The positive and negative values of the K parameters correspond to an increase or decrease in magnetic permeability in the x or y direction. For example, the parameter K_{40} for m_1 is negative, which means that the permeability in this direction is reduced and it is more difficult

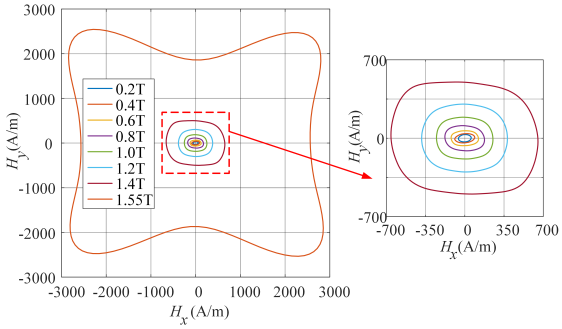

Fig. 6. Measured $\boldsymbol{H}$ loci under circular $\boldsymbol{B}$ ($\boldsymbol{B}_{\mathrm{p}}$=0.2-1.55 T).

to magnetize. The parameter K_{04} for m_2 is positive, which means that the permeability in this direction increases, making magnetization easier. K_{40} and K_{04} are the lowest powers of m_1 and m_2, so their proportion in the anisotropic field is the highest. Their positive and negative values can be determined by the sample properties obtained through measurement. For other K parameters, their signs are uncertain.

It is worth noting that this model within the EB model framework is very simple in simulating the irreversible field $\boldsymbol{H}_{\mathrm{ir}}$. The integration of $\boldsymbol{H}$ and $\boldsymbol{B}$ is the loss

$$W = \int_T \left(H_x \frac{dB_x}{dt} + H_y \frac{dB_y}{dt} \right) dt. \tag{19}$$

The accurate prediction of hysteresis loss is closely related to the irreversible field. By using the hysterons shown in Fig. 3 with different major axis κ, it is possible to accurately simulate shapes and alternating losses of hysteresis loops with different sizes in a single direction. However, the anisotropy of the irreversible field changes with the increase of magnetization, that is, for hysterons with different κ, its axial ratio L and rotation angle θ also change. If this feature is considered, the probability densities function $\boldsymbol{p}$ should contain three independent variables, and the number of hysterons will increase significantly, which greatly increases the complexity of the model. This paper aims to provide an easy-to-implement model, so only the change of κ is considered. Meanwhile, to get a relatively accurate loss prediction result, the definition of the error function includes the components of $\boldsymbol{B}$ and W:

$$\begin{aligned} \varepsilon_{\mathrm{f}} = & \frac{1}{N_{\mathrm{g}} N_{\mathrm{d}}} \sum_{j=1}^{N_{\mathrm{g}}} \sum_{i=1}^{N_{\mathrm{d}}} \frac{\left\| \boldsymbol{B}_{\mathrm{m}}^{i,j} - \boldsymbol{B}_{\mathrm{c}}^{i,j} \right\|}{\boldsymbol{B}_{\max}} \cdot \xi \\ & + \frac{1}{N_{\mathrm{g}}} \sum_{j=1}^{N_{\mathrm{g}}} \frac{\left| W_{\mathrm{m}}^{j} - W_{\mathrm{c}}^{j} \right|}{\left| W_{\mathrm{m}}^{j} \right|} \cdot (1 - \xi) \end{aligned} \tag{20}$$

There are N_{g} groups of measured data participating in the identification, and each group contains N_{d} data points. $\boldsymbol{B}_{\mathrm{m}}$ and $\boldsymbol{B}_{\mathrm{c}}$ are the measured and calculated magnetic flux density, respectively. $\boldsymbol{B}_{\max}$ is max flux density of the measurements, which is used to transfer the error of $\boldsymbol{B}$ value into a percentage. W_{m} and W_{c} are the measured and calculated loss, respectively. ξ is the weight coefficient between $\boldsymbol{B}$ error and W error, taken as 0.5 in this study.

In the next subsections, the effect of the datasets used in the identification procedure on the output of the model

Name	Unit	Value
K_{40}^{A}	J/m^3	-64.3
K_{04}^{A}	J/m^3	197.8
K_{22}^{A}	J/m^3	92.3
K_{60}^{A}	J/m^3	25.5
K_{06}^{A}	J/m^3	-44.3
K_{42}^{A}	J/m^3	135.7
K_{24}^{A}	J/m^3	-1.9
a_1^{A}	A/m	211.2
a_2^{A}	A/m	39.8
M_S^{A}	MA/m	1.4
ω^{A}	-	6.2×10^{-1}
C_1^{A}	A/m	-127.1
C_2^{A}	A/m	121.2
L^{A}	-	8.7×10^{-1}
θ^{A}	deg.	20.1
η^{A}	-	8.7×10^{-1}

(a)

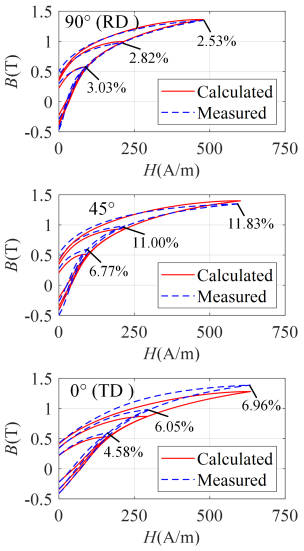

(b)

Fig. 7. Results of parameters identification using set (A). (a) Table of parameters. (b) Comparison between the measured hysteresis loops and the ones calculated by the proposed model with these parameters.

from both the ***BH***-characteristics and the hysteresis losses are investigated. For this purpose, either the alternating measurement data (A) or the rotational measurement data (R) is used and the behaviour of the model under the other loading mode, i.e. (R) or (A) is analyzed respectively. On the one hand, the identification can be carried out either separately for the anhysteretic and hysteretic parameters, or simultaneously for all the parameters. The separate identification procedure is computationally efficient, but the interaction between the parameters requires that they are identified simultaneously. On the other hand, parameters of the model are not unique and the error function may have multiple minimum points. To reduce the computation time and better demonstrate the differences in the identification results between the two datasets, the initial values for the identification of them are set to the parameters identified separately with rotational measurements. For both identification procedures, the sequential quadratic programming algorithm is adapted.

1) Identify parameters from set (A): The identified parameters from the set (A) are shown in Fig. 7. The fitting error in this case is 4.73 %. The error of each alternating hysteresis loop is shown in Fig. 7. These results show, the fitting results are well and the proposed model describes very well the anisotropy of the material.

Fig. 8 shows the comparison between the predicted core losses and the measured ones of different values of the pick flux density B_p. Compared with the loss value of 2.1 W/kg at a magnetic density amplitude of 1.5 T at 50 Hz provided by the manufacturer, the predicted loss in the rolling direction is 1.43 W/kg. In this paper, one of set (A) and (R) is used to identify model parameters and the other dataset is used to verify the model. For the rotational tester, it had been studied that the error of the magnetic field and magnetic flux density are higher than 9.1% and 7%, respectively [28]. Therefore, the measured loss calculated by (19) can be approximately regarded as the sum of these errors, namely 16%. According

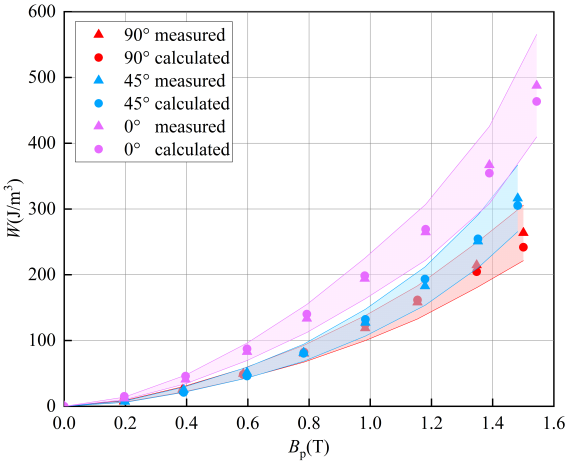

Fig. 8. Comparison between the measured and calculated alternating losses (model parameters identified by the set (A)). The shaded area represents the error margin related to the measured quantities.

Name	Unit	Value
K_{40}^{R}	J/m^3	-46.6
K_{04}^{R}	J/m^3	200.8
K_{22}^{R}	J/m^3	78.4
K_{60}^{R}	J/m^3	60.6
K_{06}^{R}	J/m^3	-32.7
K_{42}^{R}	J/m^3	129.0
K_{24}^{R}	J/m^3	-14.2
a_1^{R}	A/m	204.7
a_2^{R}	A/m	54.2
M_S^{R}	MA/m	1.3
ω^{A}	-	5.0×10^{-1}
C_1^{R}	A/m	-124.2
C_2^{R}	A/m	144.9
L^{R}	-	4.9×10^{-1}
θ^{R}	deg.	18.9
η^{R}	-	8.8×10^{-1}

(a)

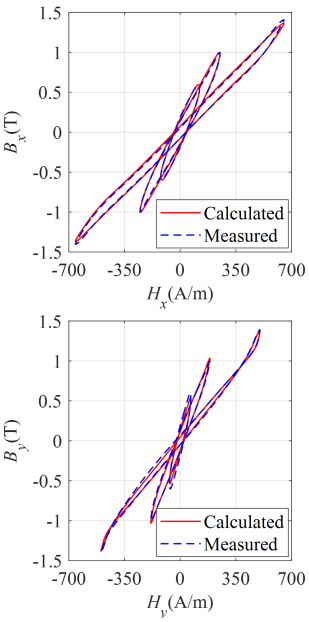

(b)

Fig. 9. Results of parameters identification using set (R). (a) Table of parameters. (b) Comparison between the measured vector magnetic properties and the ones calculated by the proposed model with these parameters. Error of each vector loci: 4.95% for B_p=0.6T, 2.91% for B_p=1.0T and 2.73% for B_p=1.4T.

to that, the shaded areas of the error bands are added in Fig. 8 and the following figures of loss comparison to evaluate the performance of the model.

2) Identify parameters from set (R): The identified parameters from the set (R) are shown in Fig. 9 and the fitting error in this case is 4.18 %. The error of each vector loci is labeled in the figure title. The calculated rotational magnetic properties show good agreement with the measured results over a wide range of the pick flux density $\boldsymbol{B}_p$. Fig. 10 shows the comparison between the predicted core losses and the measured ones. The coherent rotation effect that makes the rotational loss drop at high values of the flux density is characterized well by the proposed model.

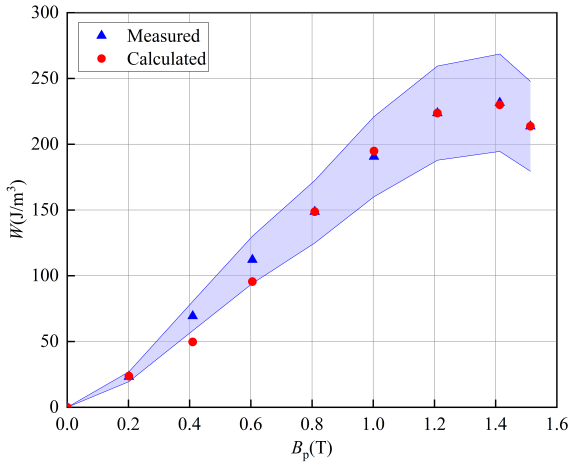

Fig. 10. Comparison between the measured and calculated rotational losses (model parameters identified by the set (R)).

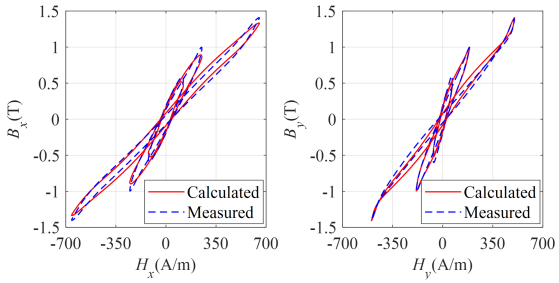

Fig. 11. Comparison between the measured vector magnetic properties and the ones calculated by the proposed model (model parameters identified by the set (A)). Error of each vector loci: 6.87% for B_p=0.6T, 5.29% for B_p=1.0T and 6.17% for B_p=1.4T.

B. Validation

In the above presented results, the same dataset is used for both the identification of the parameters, which are applied to the simulation of the corresponding measurements. Thus the good match between the measurements and the modeling is not that surprising, but it serves to confirm the quality of the model through the fitting procedure. To validate the model, the parameters identified from one dataset are used to simulate the other dataset.

1) Validate model by set (R): With parameters in Fig. 7, the predicted vector magnetic properties are shown in Fig. 11 and the fitting error is 10.22 %. Fig. 12 shows the comparison results of the losses. The shapes of *Hx-Bx* and *Hy-By* are not predicted perfectly, whereas the calculated losses still have a good tendency with the measured ones. The error is relatively large when the $\boldsymbol{B}_p$ is larger than 1.0 T. In general, the amplitude of $\boldsymbol{B}$ is predicted well but some errors exist in the orientation of $\boldsymbol{B}$.

2) Validate model by set (A): With parameters in Fig. 9, the predicted alternating hysteresis loops are shown in Fig. 13 and the fitting error is 10.93 %. Fig. 14 shows the comparison results of the losses. The slopes of the hysteresis loops under different directions of magnetization are simulated, but the coercive field is lower than the measured coercive field, resulting in losses that are lower than the measured losses when the $\boldsymbol{B}_p$ is higher than 1.0 T.

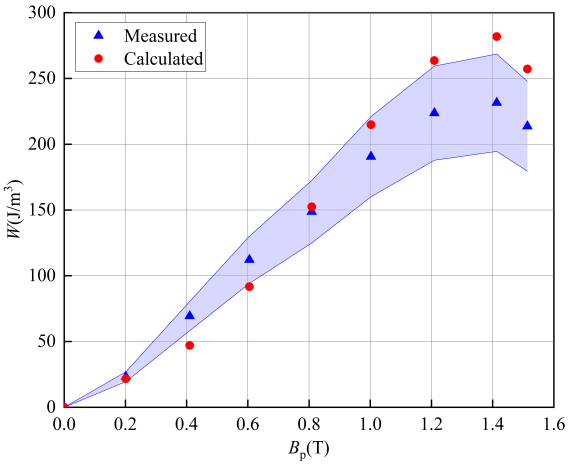

Fig. 12. Comparison between the measured and calculated rotational losses (model parameters identified by the set (A)).

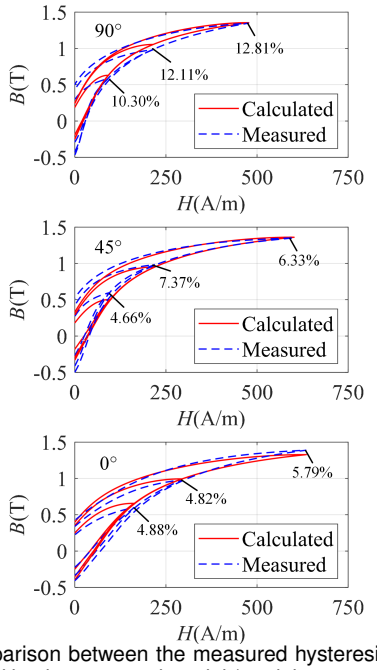

Fig. 13. Comparison between the measured hysteresis loops and the ones calculated by the proposed model (model parameters identified by the set (R)).

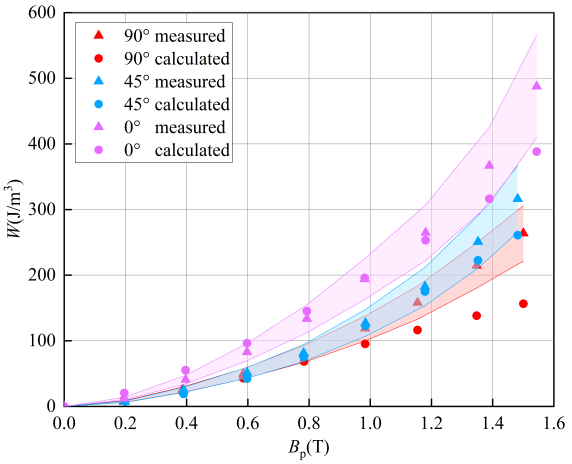

Fig. 14. Comparison between the measured and calculated alternating losses (model parameters identified by the set (R)).

3) Analysis: Based on the above results, it can be seen that if set (A) is used to predict set (R), the rotation losses are greater than the measured values when the $\boldsymbol{B}_p$ is greater than 1.0 T; if set (R) is used to predict set (A), the alternating losses are lower than the measured values when the $\boldsymbol{B}_p$ is greater than 1.0 T. By comparing the tables in Fig. 7 and Fig. 9, it can be found that there is little difference in the dominant parameters K_{40}, K_{04} and K_{22} that characterize anisotropy of the reversible magnetization, and the parameters a_1, a_2, M_{S} and ω that describe the anhysteretic curve are also very similar. Therefore, no matter which dataset is used to identify parameters, the shape of the alternating loops or rotational loci is always accurate, such as the inclination of the alternating loops. However, there are significant differences in L between the two sets of parameters, namely 0.87 and 0.49. In the identification section, it is described that the L characterizes the anisotropy of the irreversible magnetization of the material, which directly affects the loss. This phenomenon can be explained by magnetic domain theory. When the magnetic density is small, the main source of hysteresis loss is domain wall motion. This is true for both alternating magnetization and rotational magnetization, so the mutual verification of losses before 1.0 T is more accurate. Whereas, as the magnetic density increases, the magnetic domains begin to merge and become larger, resulting in a decrease in the number of domain walls. The remaining few large magnetic domains rotate with the applied field. The proportion of domain rotation in rotational magnetization is greater than that in alternating magnetization. Therefore, after 1.0 T, the alternating parameters overestimate the rotational loss, while the rotational parameters underestimate the alternating loss.

Besides, the alternating losses are obtained with a single measured loop. However, the rotational losses are obtained with two measured loops, one rotating clockwise and one rotating counter-clockwise. Hence, the rotational losses also carry higher measurement error than the alternating loss and require good reproducibility with a perfectly sinusoidal signal. Finally, the excess losses are also different for the rotating flux density and alternating flux density, which may also be one of the error sources.

Theoretically, identifying parameters with rotational magnetic properties allows for considering all magnetization directions. Thus, the vector magnetic properties can be predicted more accurately. For electrical equipment such as rotational machines that work under rotational magnetization, the simulation accuracy can be improved compared with modeling using alternating magnetic properties. However, due to its complexity and error sensitivity, the vector magnetic properties tester does not have a standard [29]. There are measurement standards for testing alternating magnetic properties, and material manufacturers even directly provide such data to users. Therefore, identifying model parameters using alternating magnetic properties has broad applicability. The proposed model can realize the prediction of vector magnetic properties only by using the alternating data in three directions, and it can still simulate the trend of loss reduction caused by coherent rotation under rotational magnetization. Considering the prediction accuracy of the model and the difficulty of obtaining measured data, we suggest using the data of alternating measurements to identify the parameters of the proposed model. However, with the development of magnetic measurement, this model can simulate the vector magnetic properties more accurately when a unified measurement standard for the rotational magnetic properties is formed in the future.

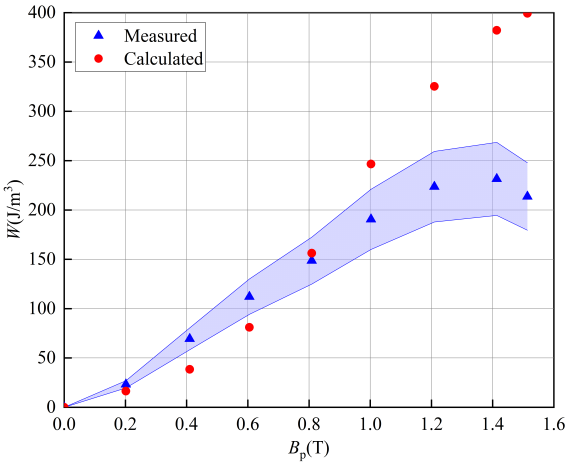

Fig. 15. Comparison between the measured and calculated rotational losses of the original EB model (model parameters identified by the set (A)).

C. Comparison with the original EB model

Remove all extensions made to the EB model in this paper to demonstrate the effective characterization of anisotropy by the proposed method. That is, all K parameters are 0, the single Langevin function (11) (excluding a_2 and ω), the circular operator ($L = 1$ and $\theta = 0$), and the F function in (17) is 0. The definition of hysteron range and distribution remains unchanged. The remaining parameters are only a_1, M_{S}, C_1, and C_2. Using set (A) to identify the parameters: $a_1 = 96.4$ A/m, $M_{\mathrm{S}} = 1.4$ MA/m, $C_1 = -135.0$ A/m, $C_2 = 78.6$ A/m, and the fitting error is 13.67 %. Verify the original EB model by set (R), as shown in Fig. 15. Comparing these results with Fig. 12, it can be seen that the proposed model significantly improves prediction accuracy and has the ability to predict the decreasing trend of rotational loss.

IV. Generality of the Proposed Model

A. Continuous angles

The model can reproduce the material behavior of any alternating directions. For example, define the model input as an alternating sine H with an amplitude of 500 A/m and an angle from the RD as the model input, the predicted results are shown in Fig. 16.

B. Another material

The rotational measurements of non-oriented electrical steel sheets M400-50A is used to verify the effect of the model for different materials, and the RD of this material was defined as the x-axis in the measurements [30]. The fitting error is 6.68 %, as shown in Fig. 17. The x-axis of B35A210 studied in this paper is the TD, its K_{40} in Fig. 9 is negative, K_{04} is positive, and L is less than 1. Conversely, the x-axis of M400-50A is

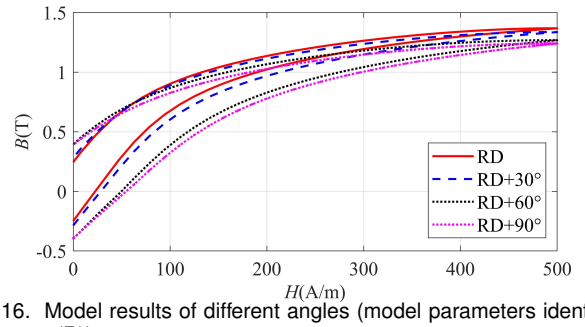

Fig. 16. Model results of different angles (model parameters identified by the set (R)).

Name	Unit	Value
K_{40}^{R}	J/m^3	110.5
K_{04}^{R}	J/m^3	-138.2
K_{22}^{R}	J/m^3	54.0
K_{60}^{R}	J/m^3	-31.1
K_{06}^{R}	J/m^3	-49.9
K_{42}^{R}	J/m^3	31.8
K_{24}^{R}	J/m^3	35.3
a_1^{R}	A/m	60.4
a_2^{R}	A/m	8.8
M_S^{R}	MA/m	1.1
ω^{A}	-	4.3×10^{-1}
C_1^{R}	A/m	-12.0
C_2^{R}	A/m	94.2
L^{R}	-	2.1
θ^{R}	deg.	30.5
η^{R}	-	9.9×10^{-1}

(a)

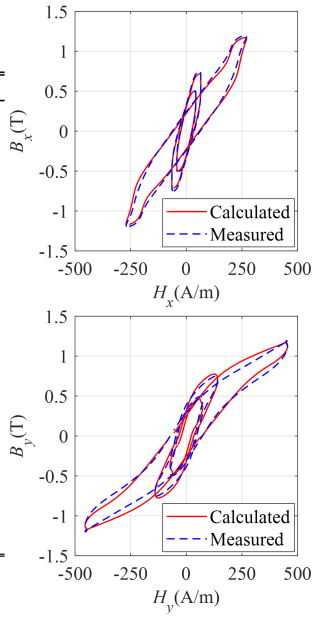

(b)

Fig. 17. Results of parameters identification for M400-50A under rotational magnetization. (a) Table of parameters. (b) Comparison between the measured vector magnetic properties and the ones calculated by the proposed model with these parameters. Error of each vector loci: 8.30% for B_p=0.5T, 5.49% for B_p=0.75T and 5.83% for B_p=1.2T.

the RD, so its K_{40} is positive, K_{04} is negative, and L is larger than 1. The discrepancies of C_1, C_2 and θ reflect the different distribution patterns of magnetic domains in the two samples.

V. Discussion and Conclusion

This paper benefits from the crystal energy theory and the EB model to propose an anisotropic vector hysteresis model. With proper coordinate transformation, the single crystal energy leads to the expression of the anisotropic energy of the magnetized sample. Moreover, the EB model is improved by replacing the applied field with the effective field to consider material anisotropy. The vector hysteresis model requires 16 parameters that can be identified from the alternating or rotational flux density measurements. The remaining set of measurements is involved to validate the model. This validation leads to an overall average error below 11%. The maximum discrepancy occurs when using set (R) to verify the loss of set (A), reaching 41% when $\boldsymbol{B}_p$ is 1.55 T. Finally, the proposed vector hysteresis model can reproduce and forecast the anisotropic properties and the losses of electrical steel sheets over a wide range of rotational and alternating excitations.

This model has a physical foundation, and in addition to the anisotropy included in this paper, it can also be further extended based on crystal energy in the future, such as a model considering mechanical stress. Only alternating data are demanded to predict rotational magnetic properties, which makes the model more applicable. Compared with the original EB model, this model is more complicated but reduces the error more than 3 times. It is also capable of predicting the magnetic properties under excitation of any angles and other non-oriented electrical sheets material.

This version of model is rate-independent and suitable for static or quasi-static magnetization. In finite element analysis (FEA), the interdependence of hysteresis and eddy currents needs to be considered. This model is compatible with fixed point formulation $\boldsymbol{H}$-ϕ or $\boldsymbol{T}$-Ω [31], [32]. The Jacobian d$\boldsymbol{B}$/d$\boldsymbol{H}$ could also be determined numerically by the model with a small field variation. Hence, this model is compatible with the Newton formulation. In addition, although the eddy current in core lamination is intrinsically a 3D problem, one feasible way to consider eddy current in 2D FEA is also investigated by other researchers [33], [34] and these methods are also available to this model.

References

[1] H. Vansompel, P. Sergeant, L. Dupre, and A. V. den Bossche, "Axial-flux pm machines with variable air gap," *IEEE Trans. Ind. Electron.*, vol. 61, no. 2, pp. 730–737, Feb. 2014.

[2] S. Zhu, M. Cheng, J. Dong, and J. Du, "Core loss analysis and calculation of stator permanent-magnet machine considering dc-biased magnetic induction," *IEEE Trans. Ind. Electron.*, vol. 61, no. 10, pp. 5203–5212, Oct. 2014.

[3] S. Steentjes, K. Hameyer, D. Dolinar, and M. Petrun, "Iron-loss and magnetic hysteresis under arbitrary waveforms in no electrical steel: a comparative study of hysteresis models," *IEEE Trans. Ind. Electron.*, vol. 64, no. 3, pp. 2511 – 2521, Mar. 2017.

[4] I. Mayergoyz, *Mathematical models of hysteresis and their applications*. USA: Elsevier, 2003.

[5] E. Dlala, A. Belahcen, K. A. Fonteyn, and M. Belkasim, "Improving loss properties of the mayergoyz vector hysteresis model," *IEEE Trans. Mag.*, vol. 46, no. 3, pp. 918–924, Mar. 2010.

[6] S. Yue, P. I. Anderson, Y. Li, Q. Yang, and A. Moses, "A modified inverse vector hysteresis model for nonoriented electrical steels considering anisotropy for fea," *IEEE Trans. Energy Convers.*, vol. 36, no. 4, pp. 3251–3260, Dec. 2021.

[7] C. Serpico, M. d'Aquino, C. Visone, and D. Davino, "A new class of preisach-type isotropic vector model of hysteresis," *Phys. B Condens. Matter*, vol. 343, pp. 117–120, 2004.

[8] G. R. Kahler, E. D. Torre, and E. Cardelli, "Implementation of the preisach-stoner-wohlfarth classical vector model," *IEEE Trans. Mag.*, vol. 46, no. 1, pp. 21–28, Jan. 2010.

[9] W. Xu, N. Duan, S. Wang, Y. Guo, and J. Zhu, "Modeling and measurement of magnetic hysteresis of soft magnetic composite materials under different magnetizations," *IEEE Trans. Ind. Electron.*, vol. 64, no. 3, pp. 2459–2467, Mar. 2017.

[10] Z. Li, J. Shan, and U. Gabbert, "Development of reduced preisach model using discrete empirical interpolation method," *IEEE Trans. Ind. Electron.*, vol. 65, no. 10, pp. 8072–8079, Oct. 2018.

[11] J. Zeng, Y. Guo, and J. Zhu, "Investigation and simulation on magnetic hysteresis properties of magnetorheological fluid," *IEEE Trans. Ind. Electron.*, vol. 64, no. 2, pp. 1611–1616, Feb. 2017.

[12] E. Cardelli, E. D. Torre, and A. Faba, "Analysis of a unit magnetic particle via the dpc model," *IEEE Trans. Mag.*, vol. 45, no. 11, pp. 5192–5195, Nov. 2009.

[13] D. Vanoost, S. Steentjes, J. Peuteman, G. Gielen, H. D. Gersem, and D. Pissoort, "Magnetic hysteresis at the domain scale of a multi-scale material model for magneto-elastic behaviour," *J. Magn. Magn. Mater.*, vol. 414, pp. 168–179, 2016.
[14] L. Daniel, O. Hubert, N. Buiron, and R. Billardon, "Reversible magneto-elastic behavior: a multiscale approach," *J. Mech. Phys. Solids*, vol. 56, no. 3, pp. 1018–1042, Mar. 2008.
[15] M. Enokizono, "Vector magnetic property and magnetic characteristic analysis by vector magneto-hysteretic e&s model," *IEEE Trans. Mag.*, vol. 45, no. 3, pp. 1148–1153, Mar. 2009.
[16] T. Pera, F. Ossart, and T. Waeckerle, "Field computation in non linear anisotropic sheets using the coenergy model," *IEEE Trans. Mag.*, vol. 29, no. 6, pp. 2425–2427, Nov. 1993.
[17] Z. Yang, C. Sun, X. Sun, and Y. Sun, "An improved dynamic model for bearingless induction motor considering rotor eccentricity and load change," *IEEE Trans. Ind. Electron.*, vol. 69, no. 4, pp. 3439–3448, Apr. 2022.
[18] B. Upadhaya, F. Martin, P. Rasilo, P. Handgruber, A. Belahcen, and A. Arkkio, "Modelling anisotropy in non-oriented electrical steel sheet using vector jiles-atherton model," *COMPEL-Int. J. Comput. Math. Electr. Electron. Eng.*, vol. 36, no. 3, pp. 764–773, May. 2017.
[19] W. Li, I. H. Kim, S. M. Jang, and C. S. Koh, "Hysteresis modeling for electrical steel sheets using improved vector jiles-atherton hysteresis model," *IEEE Trans. Mag.*, vol. 47, no. 10, pp. 3821 – 3824, Oct. 2011.
[20] A. Bergqvist, "Magnetic vector hysteresis model with dry friction-like pinning," *Phys. B Condens. Matter*, vol. 233, pp. 342–347, Jun. 1997.
[21] F. Henrotte, A. Nicolet, and K. Hameyer, "An energy-based vector hysteresis model for ferromagnetic materials," *COMPEL-Int. J. Comput. Math. Electr. Electron. Eng.*, vol. 25, no. 1, pp. 71–80, Jan. 2006.
[22] B. Upadhaya, P. Rasilo, L. Perkkio, P. Handgruber, A. Belahcen, and A. Arkkio, "Comparison of anisotropic energy-based and jiles-atherton models of ferromagnetic hysteresis," *IEEE Trans. Mag.*, vol. 56, no. 4, p. Art. no. 7300307, Apr. 2020.
[23] S. Steentjes, F. Henrotte, and K. Hameyer, "Energy-based ferromagnetic material model with magnetic anisotropy," *J. Magn. Magn. Mater.*, vol. 425, pp. 20–24, Mar. 2017.
[24] B. Ducharne, S.Zurek, and G.Sebald, "A universal method based on fractional derivatives for modeling magnetic losses under alternating and rotational magnetization conditions," *J. Magn. Magn. Mater.*, vol. 550, p. Art. no. 169071, Apr. 2022.
[25] F. Martin, U. Aydin, A. Ruzibaev, Y. Ge, L. Daniel, L. Bernard, P. Rasilo, A. Benabou, and A. Belahcen, "Analysis of the magneto-mechanical anisotropy of steel sheets in electrical applications," *IEEE Trans. Mag.*, vol. 56, no. 2, p. Art. no. 7509804, Feb. 2020.
[26] A. Hubert and R. Schäfer, *Magnetic Domains: The Analysis of Magnetic Microstructures*, 3rd ed. New York: Springer Science & Business Media, 2009, pp. 138-140.
[27] S. Steentjes, M. Petrun, G. Glehn, D. Dolinar, and K. Hameyer, "Suitability of the double langevin function for description of anhysteretic magnetization curves in no and go electrical steel grades," *AIP Advances*, vol. 7, no. 5, p. Art. no. 056013, May. 2017.
[28] S. Zurek, "Two-dimensional magnetisation problems in electrical steels," Ph.D. dissertation, Cardiff University, Wales, United Kingdom, Mar. 2005. [Online]. Available: https://orca.cardiff.ac.uk/id/eprint/55978/1/U584713.pdf
[29] C. Zhang, Y. Li, J. Li, Q. Yang, and J. Zhu, "Measurement of three-dimensional magnetic properties with feedback control and harmonic compensation," *IEEE Trans. Ind. Electron.*, vol. 64, no. 3, pp. 2476–2485, Mar. 2017.
[30] U. Aydin, F. Martin, P. Rasilo, A. Belahcen, A. Haavisto, D. Singh, L. Daniel, and A. Arkkio, "Rotational single sheet tester for multiaxial magneto-mechanical effects in steel sheets," *IEEE Trans. Mag.*, vol. 55, no. 3, p. Art. no. 2001810, Mar. 2019.
[31] K. Jacques, "Energy-based magnetic hysteresis models-theoretical development and finite element formulations," Ph.D. dissertation, Free University of Brussels, Brussels, Belgium, Nov. 2018. [Online]. Available: https://orbi.uliege.be/bitstream/2268/229596/1/JACQUES_Kevin_thesis-20181123.pdf
[32] M. Kuczmann and A. Iványi, *The Finite Element Method in Magnetics*. Hungary: Academic, 2008.
[33] O. Bottauscio, M. Chiampi, and D. Chiarabaglio, "Advanced model of laminated magnetic cores for two-dimensional field analysis," *IEEE Trans. Mag.*, vol. 36, no. 3, pp. 561–573, May. 2000.
[34] E. Dlala, A. Belahcen, and A. Arkkio, "Efficient magnetodynamic lamination model for two-dimensional field simulation of rotating electrical machines," *J. Magn. Magn. Mater.*, vol. 320, pp. e1006–e1010, 2008.

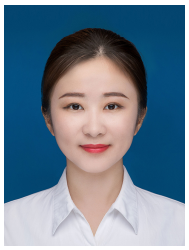

Ruiying Chen was born in Hebei, China, in 1995. She received the B.E. degree in electrical engineering and automation from Liaoning Technical University, Huludao, China, in 2017. Since 2017, she has been studying for Master and Ph.D. degrees in electrical engineering with the Hebei University of Technology, Tianjin, China.

As a Visiting Doctoral Student, she visited Aalto University, Espoo, Finland, from 12.2020 to 12.2022. Her research interests include the modeling of vector magnetic materials and the calculation of iron loss.

Floran Martin received the Engineering Diploma in electrical engineering from Polytech Nantes, Nantes, France, in 2009, and the M.S. and Ph.D. degrees in electrical engineering from the University of Nantes, Nantes, in 2009 and 2013, respectively.

In 2014, he joined the Department of Electrical Engineering and Automation, Aalto University, Espoo, Finland, where he is currently a Staff Scientist. His research interests include modeling of magnetic materials as well as analyzing, designing, and controlling electrical machines.

Yongjian Li was born in Hebei, China, in 1978. He received the B.Eng., M.Eng., and Ph.D. degrees from the Hebei University of Technology, Tianjin, China, in 2002, 2007, and 2011, respectively.

From 2009 to 2011, he was a Research Assistant at UTS, Australia. As a visiting scholar, he visited Ottawa University, Canada from 2016 to 2017. He is now the Associate Dean of Electrical Engineering School, Hebei University of Technology as a Full Professor since 2015. He is member of International COMPUMAG Society and board member of International Steering Committee of 1&2-Dimensional Magnetic Measurement and Testing Workshop. His research interests include computational electromagnetics, measurements and modelling of magnetic properties, high frequency transformers.

Shuaichao Yue was born in Hebei, China, in 1992. He received B.Eng., M.Eng. and Ph.D. degrees in electrical engineering from Hebei University of Technology, Tianjin, China, in 2016, 2018 and 2023, respectively.

He was a visiting researcher of Wolfson Centre for Magnetics, Cardiff University from 2019 to 2021. He is now a postdoc at Hebei University of Technology. His current research interests include the measurement of magnetic properties, hysteresis modelling and its application.

Anouar Belahcen (M'13-SM'15) was born in Morocco in 1963. He received the M.Sc. (Tech.) and Doctor (Tech.) degrees from Aalto University (former Helsinki University of Technology), Finland, in 1998, and 2004, respectively.

He is now Professor of Power and Energy at Aalto University, Finland. His research interest are numerical modelling of electrical machines, characterization and modelling of magnetic materials, coupled magneto-mechanical problems, magnetic forces, magnetostriction, and fault diagnostics of electrical machines. Since 2020, Anouar Belahcen is the vice dean for education at the school of Electrical Engineering at Aalto University, and since 2022 he is the director of the Academy of Finland Center of Excellence in High-Speed Electromechanical Energy Conversion Systems (HiECSs).